Supporting Information for

Thermal Desorption Bridged the Gap between Dielectric Barrier Discharge Ionization and Dried Plasma Spot Samples for Sensitive and Rapid Detection of Fentanyl Analogs in Mass Spectrometry

Dongmei Li,[ab] Zehua Li,[a] Bin Xu,[a] Jia Chen,[a] Jinjuan Xue,[a] Shundi Hu,[c] Luhong Wen,[c] Lei Guo,[*a] Jianwei Xie[a] and Guibin Jiang[b]

[a] State Key Laboratory of Toxicology and Medical Countermeasures, and Laboratory of Toxicant Analysis, Institute of Pharmacology and Toxicology, Academy of Military Medical Sciences, Beijing 100850, China

[b] State Key Laboratory of Environmental Chemistry and Ecotoxicology, Research Center for Eco-Environmental Sciences, Chinese Academy of Sciences, Beijing 100085, China

[c] The Research Institute of Advanced Technologies, Ningbo University, Ningbo, 315211, China

*To whom correspondence should be addressed.

Prof. Lei Guo

E-mail: guolei@bmi.ac.cn

Table of contents

Finite Element Simulations.

1. Geometry

A two-dimensional axisymmetric model was selected. With this, we constructed six simplified models, i.e., concave-TD, flat-TD, convex-TD, semi-covered concave-TD, semi-covered flat-TD, and semi-covered convex-TD. The models consisted of 16 mm×12 mm of the air, 16 mm×0.18 mm of a paper substrate, a concave heating source of 6 mm in diameter and 3.5 mm in-depth, and a 3.5 mm high aluminum block to form flat-TD or a 5.5 mm one to form convex-TD. Narrow strips around the models were defined as infinite element domain, which meant an open ambient. Roof-shaped borderlines were built as a semi-cover.

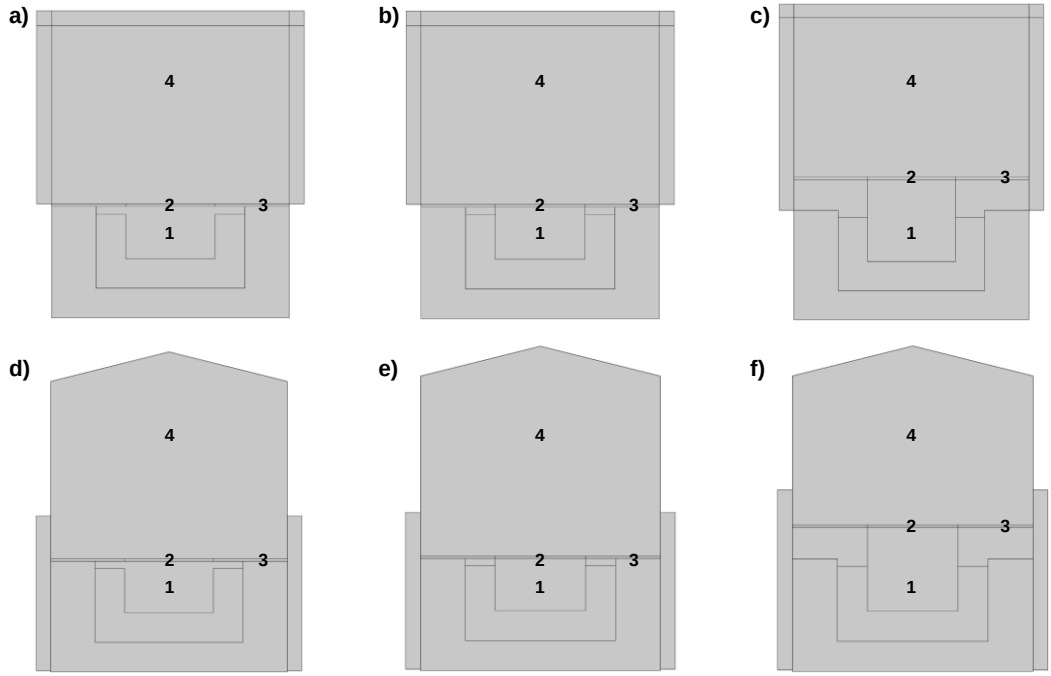

Fig. S1 Six models of concave-TD (a), flat-TD (b), convex-TD (c), semi-covered concave-TD (d), semi-covered flat-TD (e) and semi-covered convex-TD (f). Numbers in the models referred as: 1-TD; 2-sample spot; 3- paper substrate; 4-air.

2. Model equations

"Moist Air" interface, including "Heat Transfer in Moist Air" and "Moisture Transport in Air", was selected for simulations.

$$\rho C_p \frac{\partial T}{\partial t} + \rho C_p \boldsymbol{u} \cdot \nabla T + \nabla \cdot \boldsymbol{q} = Q + Q_p + Q_{vd} \quad (1)$$

$$\boldsymbol{q} = -k\nabla T \quad (2)$$

$$M_v \frac{\partial C_v}{\partial t} + M_v \boldsymbol{u} \cdot \nabla c_v + \nabla \cdot \boldsymbol{g}_w = G \quad (3)$$

$$\boldsymbol{g}_w = -M_v D \nabla c_v \quad (4)$$

$$c_v = \varphi_w c_{sat} \quad (5)$$

$$-\boldsymbol{n} \cdot \boldsymbol{g}_w = g_{evap} \quad (6)$$

$$g_{evap} = \begin{cases} M_v K(c_{sat} - c_v) & if\ c_v > c_{sat}\ or\ c_l > 0 \\ 0 & otherwise \end{cases} \quad (7)$$

Where ρ is the density, C_p is the heat capacity at constant pressure, $\boldsymbol{u}$ is the velocity vector, $\boldsymbol{q}$ is the heat flux vector, Q is the quantity of heat, k is the coefficient of thermal conductivity, M is the molar mass, c_v is the concentration of vapor, c_l is the concentration of liquid, c_{sat} is the saturation concentration, $\boldsymbol{g}_w$ presents binary diffusion, g_{evap} is the transpiration heat flux, D is the diffusion coefficient, φ_w is the relative humidity, and K is the evaporation rate factor.

3. Parameters

Initial values of ambient temperatures were defined as 20 °C, and relative humidity as 0.4. The temperature of the heating source was set at 275 °C. The evaporation rate factor was 10 m/s, and the initial liquid water concentration on a moist surface was 5 mol/m^2, calculated by the flowing formula:

$$c = \frac{\frac{\rho v}{M}}{\pi r^2} = \frac{\frac{1\ g/mL \times 2.5\ \mu L}{18\ g/mol}}{3.14 \times (0.003\ m)^2} \approx 5\ mol/m^2$$

4. Mesh

COMSOL is based on finite element analysis; therefore, mesh generation was needed. The present study used extra-fine free triangular meshes for the simulation. Mapped meshes were selected for the area of the paper substrate and infinite element domain for accurate simulation.

5. Simulation

The time-dependent simulation was adopted for investigating heat transfer from three different TD surfaces to the paper substrate, concentrations of water vapor in ionization regions, and liquid water concentrations on the paper substrate. Output times were 0 to 10 s with the step of 0.1 s.

For the simulations of using methanol as desorption solvent, modeling settings were the same as above of water, just changing the same parameters of water to that of methanol, i.e., diffusion coefficient, latent heat of phase transition, saturated vapor pressure, and molar mass.

Table S1 Box-Behnken design (BBD) factors and code levels.

Experimental factor	Symbol	levels		
		-1	0	1
Desorption solvent (H_2O:MeOH)	A	3:7	5:5	7:3
Temperature of TD (°C)	B	250	275	300
Desorption time (s)	C	6	9	12
Diameter of sample spot (mm)	D	4	5	6

Table S2 Analysis of variance (ANOVA) for response surface quadratic model of fentanyl.

Source	Sum of squares	Degree of freedom	Mean square	F-value	p-value	
Model	7.17E+09	14	5.12E+08	11.22	<0.0001**	significant
A-desorption solvent	4.85E+08	1	4.85E+08	10.63	0.0068**	
B-temperature of TD	7.24E+08	1	7.24E+08	15.87	0.0018**	
C-desorption time	8.99E+08	1	8.99E+08	19.72	0.0008**	
D-diameter of sample spot	1.92E+09	1	1.92E+09	42.04	<0.0001**	
AB	4.65E+07	1	4.65E+07	1.02	0.3327	
AC	7.68E+07	1	7.68E+07	1.68	0.2188	
AD	5.69E+08	1	5.69E+08	12.47	0.0041 **	
BC	1.71E+07	1	1.71E+07	0.37	0.5519	
BD	8.90E+07	1	8.90E+07	1.95	0.1878	
CD	8.05E+07	1	8.05E+07	1.76	0.2088	
A^2	4.40E+07	1	4.40E+07	0.96	0.3454	
B^2	1.38E+09	1	1.38E+09	30.34	0.0001**	
C^2	1.30E+07	1	1.30E+07	0.29	0.6027	
D^2	1.12E+08	1	1.12E+08	2.47	0.1424	
Residual	5.47E+08	12	4.56E+07			
Lack of Fit	4.65E+08	10	4.65E+07	1.13	0.5562	not significant
Pure Error	8.21E+07	2	4.10E+07			
Cor Total	7.71E+09	26				

**p<0.01 is extremely significant; *p<0.05 is significant.

The model F-value of 11.22 and the associated p-value of less than 0.0001 implied the model was highly significant. The F-value of the lack of fit was 1.13 (< 11.22 as a cut-off value for significance), and the p-value was 0.5562 ($p > 0.05$), which was insignificant and further indicated that the model fit well and was of statistical significance. ANOVA for the response surface linear model of other FTNs was also performed, and the influence of parameters was almost similar.

Table S3 Multiple reaction monitoring detection conditions used on Agilent 6430 QqQ-MS/MS.

Compound	Precursor ion	Product ion	Dwell (ms)	Fragmentor (V)	Collision Energy (eV)
Norfentanyl	233.2	84.1 55.1	50	110	17 40
Fentanyl	337.2	188.1 105.1	50	145	21 40
Fentanyl-D5	342.2	188.1 105.1	50	140	21 40
3-Methylfentanyl	351.2	202.1 105.1	50	150	25 40
para-Fluorofentanyl	355.2	188.1 105.1	50	155	25 40
4-Fluorobutyr fentanyl	369.2	188.1 105.1	50	155	25 40
Furanylfentanyl	375.2	188.1 105.1	50	145	21 40
Remifentanil	377.2	317.1 228.1	50	135	13 17
Sufentanil	387.2	238.1 140.1	50	130	17 25
Carfentanil	395.2	335.1 246.1	50	145	17 21

Table S4 Linearity of 8FTNs obtained by DBDI-TD-QqQ-MS/MS.

Analytes	$y = ax + b$		
	Slope a	Intercept b	R^2
Fentanyl	0.0050	−0.1996	0.9964
Norfentanyl	0.0007	−0.1279	0.9972
3-Methylfentanyl	0.0037	−0.1077	0.9965
Carfentanyl	0.0013	−0.0317	0.9906
Furanylfentanyl	0.0039	−0.0126	0.9990
para-Fluofentanyl	0.0034	−0.0304	0.9974
Sufentanil	0.0040	−0.0833	0.9928
4-Fluorobutyrfentanyl	0.0043	−0.0328	0.9981

Table S5 Matrix effects for FTNs analysis.

Compound	Concentration	Matrix effect (%) (Relative standard deviation, %, *n*=6)			
		Rat plasma	Rabbit blood	Rabbit plasma	Human plasma
Norfentanyl	Low	37.4 (18.9)	122 (19.7)	41.8 (19.7)	85.2 (18.2)
	Medium	58.6 (5.73)	129.8 (15.5)	80.9 (13.1)	131 (10.9)
	High	32.4 (12.5)	110 (16.5)	58.1 (20.3)	84.4 (10.4)
Fentanyl	Low	41.7 (9.88)	73.3 (3.32)	43.1 (18.9)	37.4 (13.5)
	Medium	49.0 (8.10)	74.1 (14.0)	34.5 (10.3)	39.0 (14.0)
	High	39.8 (8.03)	65.5 (16.4)	45.3 (9.95)	54.0 (14.4)
3-Methylfentanyl	Low	34.9 (13.5)	92.7 (11.4)	42.9 (15.5)	39.4 (20.8)
	Medium	24.0 (13.4)	69.4 (17.7)	28.4 (16.0)	41.3 (18.2)
	High	18.34 (14.1)	53.8 (16.7)	37.2 (13.9)	31.0 (19.4)
para-Fluorofentanyl	Low	46.2 (20.6)	93.0 (7.48)	50.0 (12.3)	41.7 (16.9)
	Medium	31.9 (9.58)	73.8 (17.5)	32.3 (11.4)	42.3 (9.12)
	High	30.81 (17.21)	63.9 (16.3)	41.3 (16.5)	48.3 (11.1)
4-Fluorobutyr fentanyl	Low	40.8 (13.4)	88.2 (14.1)	50.3 (14.7)	35.2 (19.8)
	Medium	30.8 (11.7)	75.3 (19.1)	34.7 (15.7)	34.9 (17.7)
	High	28.9 (14.4)	59.5 (18.9)	31.6 (13.9)	41.9 (16.9)
Furanylfentanyl	Low	81.6 (14.0)	137 (13.3)	71.7 (19.6)	72.1 (16.8)
	Medium	38.2 (13.2)	83.3 (13.6)	45.5 (3.40)	44.1 (15.6)
	High	38.9 (14.9)	66.7 (16.1)	58.8 (10.5)	65.4 (13.4)
Remifentanil	Low	--	83.2 (15.4)	38.8 (12.1)	43.7 (16.0)
	Medium	--	79.0 (19.6)	22.0 (20.3)	36.3 (16.7)
	High	--	54.5 (16.7)	22.9 (15.9)	43.9 (13.1)
Sufentanil	Low	35.7 (13.9)	101 (12.8)	42.0 (13.8)	41.8 (9.74)
	Medium	24.2 (7.64)	67.8 (11.8)	30.7 (14.9)	42.6 (9.61)
	High	16.6 (20.9)	50.2 (18.6)	27.0 (17.8)	44.7 (18.3)
Carfentanil	Low	39.8 (16.8)	107 (15.0)	81.6 (8.09)	54.3 (15.9)
	Medium	28.0 (19.8)	68.1 (15.4)	39.9 (17.6)	43.1 (12.7)
	High	21.8 (18.6)	55.7 (15.2)	46.7 (20.5)	58.0 (9.45)

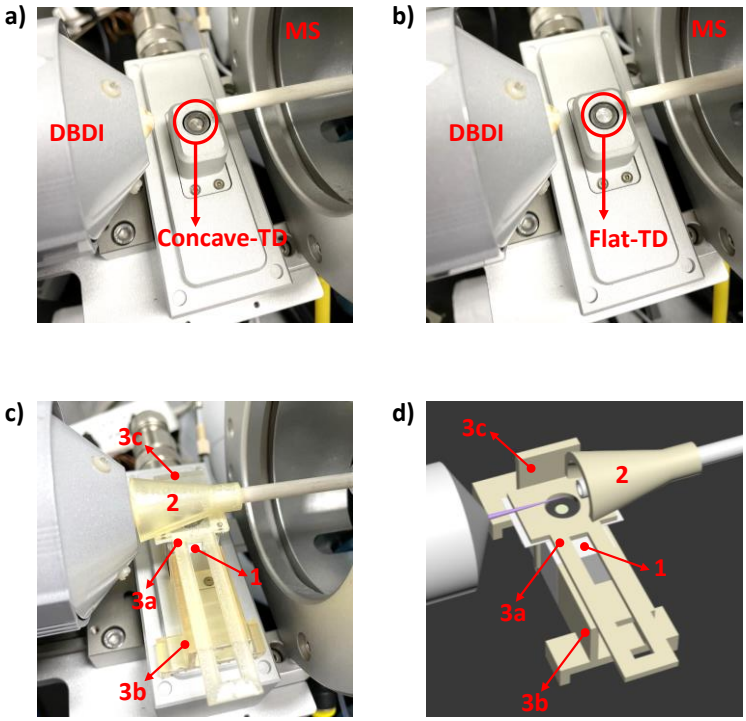

Fig. S2 Photograph of the concave-TD (a) and flat-TD device (b). Photograph (c) and three-dimensional graphics (d) of the customized semi-covered flat-TD interface. The customized interface contained (1) a flat-TD surface, (2) an ion transmission enhancer (i.e., the semi-cover), and (3) a DPS/DBS sample feeder including a sample loader (3a), a sample holder (3b), and a baffle (3c).

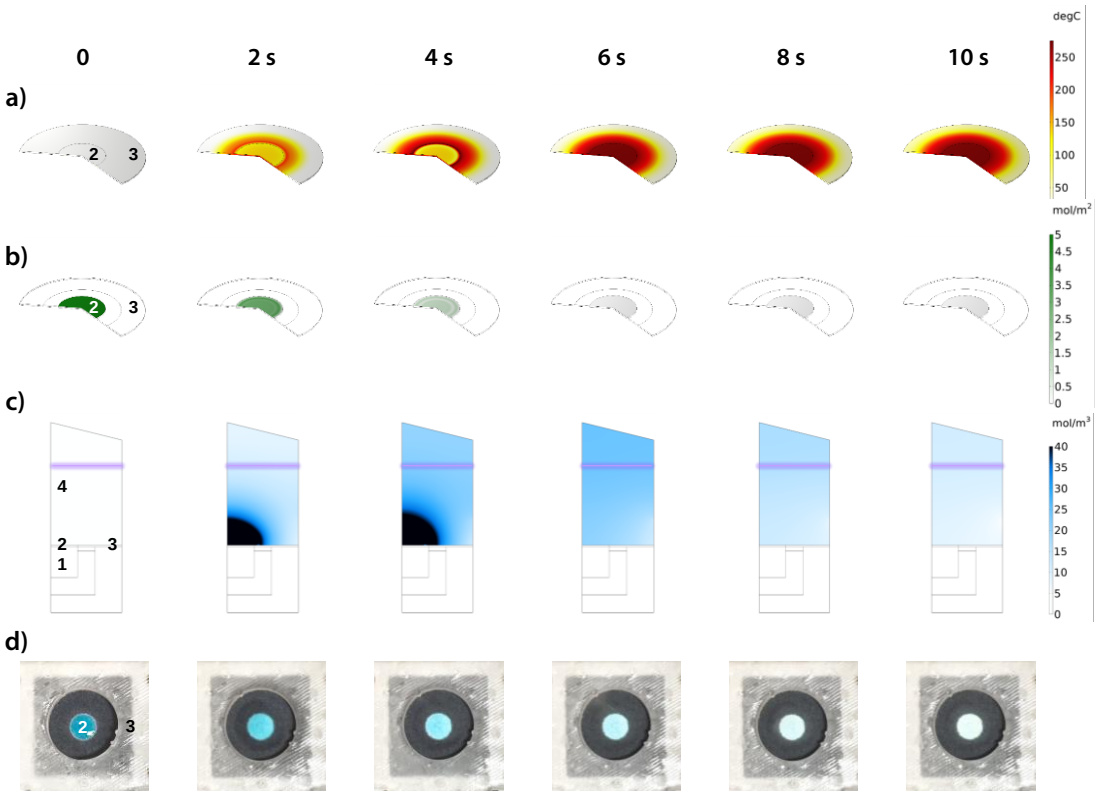

Fig. S3 Theoretical simulation of semi-covered flat-TD models using water as desorption solvent for time scale data from 0 to 10 s. Results were shown for temperature distribution (a), the concentration of water on a paper substrate (b), and in the ionization area (c). Purple lines referred to the DBD plasma torch. Numbers in the models referred to as: 1-flat-TD; 2-sample spot; 3-paper substrate; 4-air. Demonstration experiment for presenting thermal desorption procedure using 100 µg/mL malachite green solution for time scale data from 0 to 10 s (d).

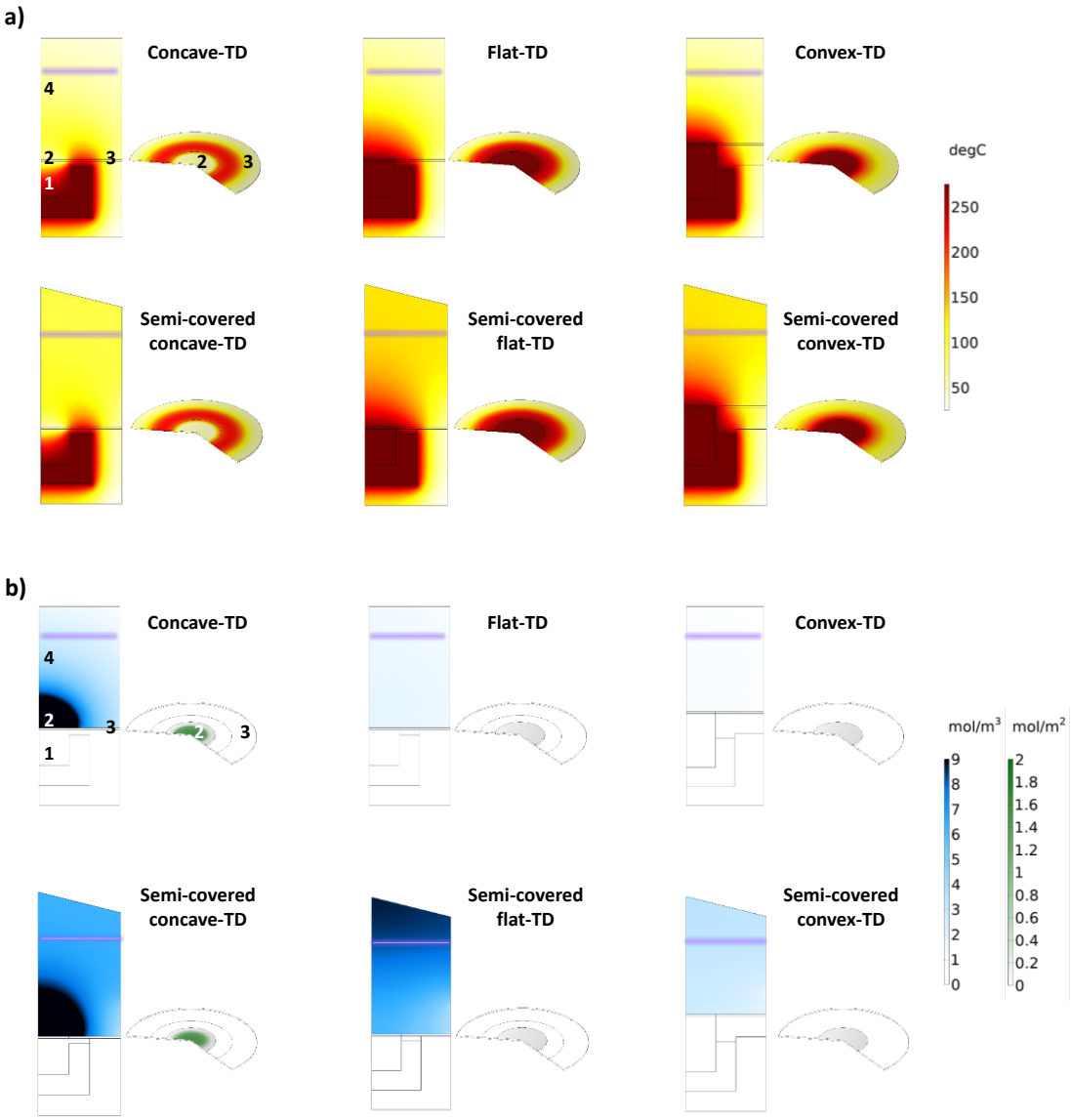

Fig. S4 Theoretical simulation of six models, concave-TD, flat-TD, convex-TD, semi-covered concave-TD, semi-covered flat-TD, and semi-covered convex-TD using methanol as desorption solvent. Results for theoretical simulation of (a) temperature distribution and (b) the water concentration on the paper substrate and in the ionization area at 10 s. Purple lines referred to the DBD plasma torch. Numbers in the models were referred to as: 1-concave-TD, flat-TD, or convex-TD; 2-sample spot; 3- paper substrate; 4-air.

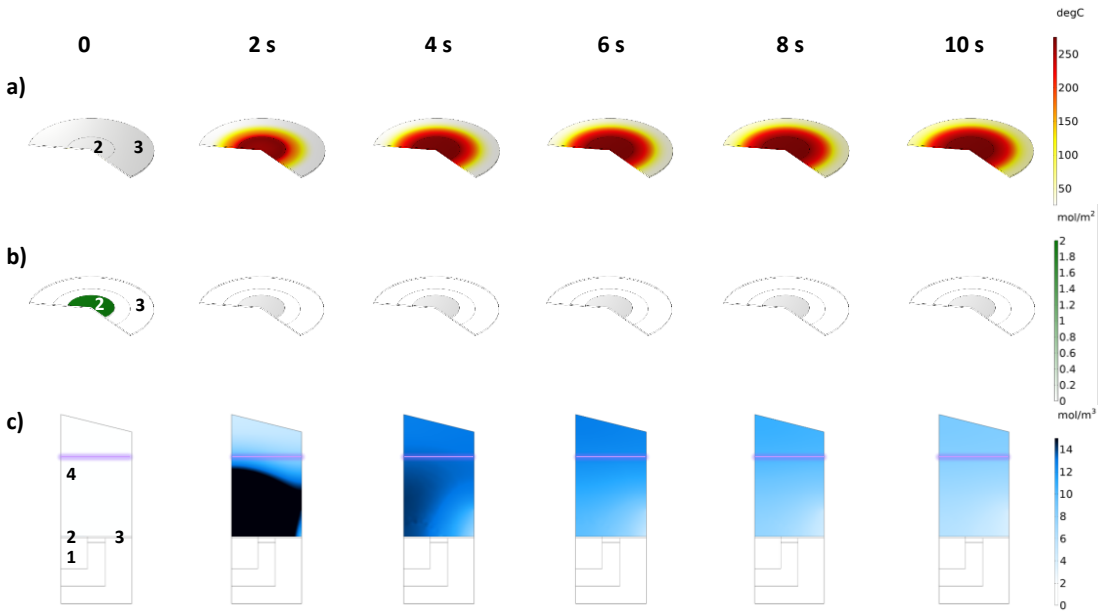

Fig. S5 Theoretical simulation of semi-covered flat-TD models using methanol as desorption solvent for time scale data from 0 to 10 s. Results were shown for temperature distribution (a), the concentration of water on a paper substrate (b), and in the ionization area (c). Purple lines referred to the DBD plasma torch. Numbers in the models referred to as: 1-flat-TD; 2-sample spot; 3- paper substrate; 4-air.

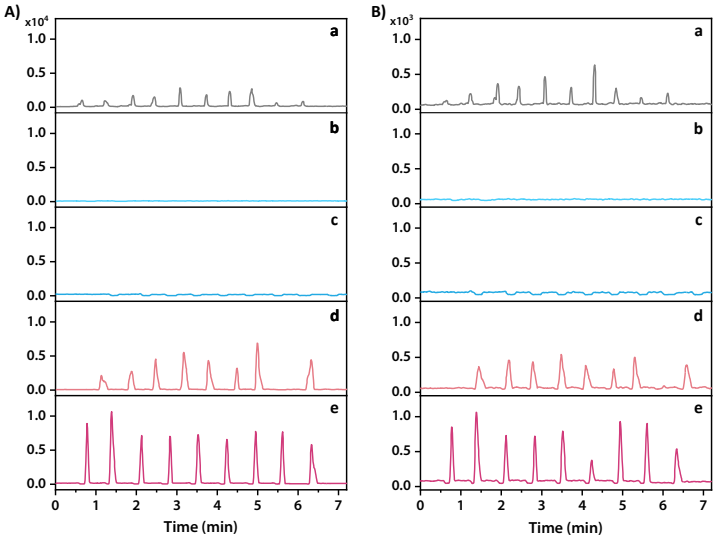

Fig. S6 Representative multiple reaction monitoring (MRM) mass chromatograms of FTNs by DBDI-TD-QqQ-MS/MS, the concentration of FTNs was 200 ng/mL. Transitions of FTNs were as follows: (A) 3-methyl fentanyl (351.2→202.1) and (B) remifentanil (377.2→228.1). Little a–e marked in the mass chromatograms corresponded to five different devices: (a) liquid sample (in a solution of methanol) as a positive control, DPS sample containing FTNs in (b) concave-TD, (c) semi-covered concave-TD, (d) flat-TD, and (e) semi-covered flat-TD.

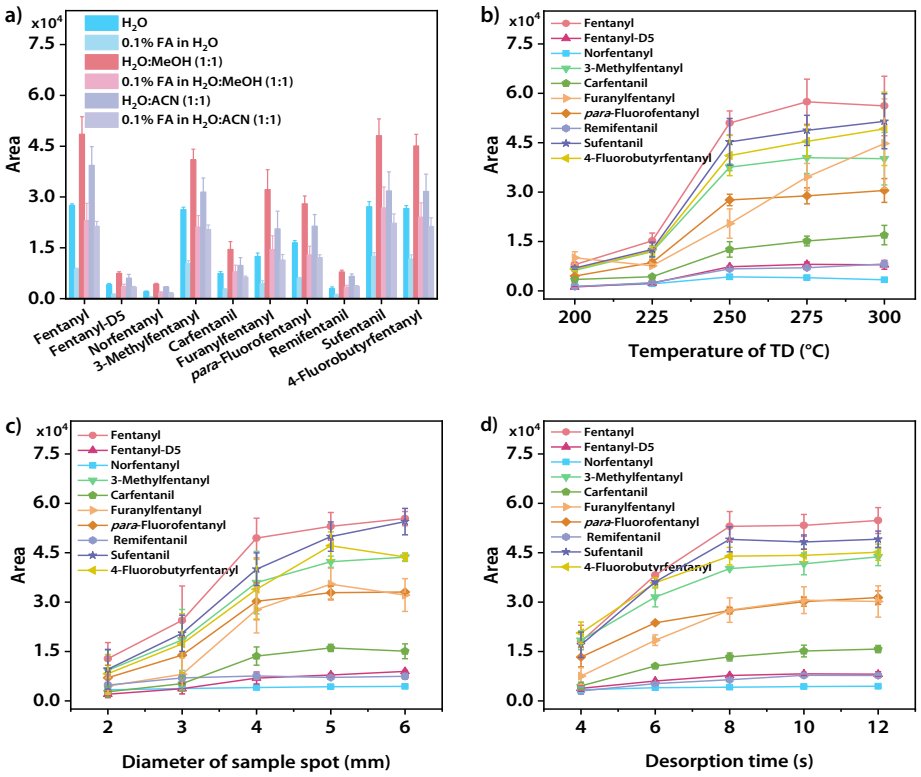

Fig. S7 Optimization of critical parameters influencing the desorption efficiency with a single factor experiment. Influences of (a) desorption solvent, (b) temperature of TD, (c) diameter of sample spot, and (d) desorption time on the peak area of FTNs.

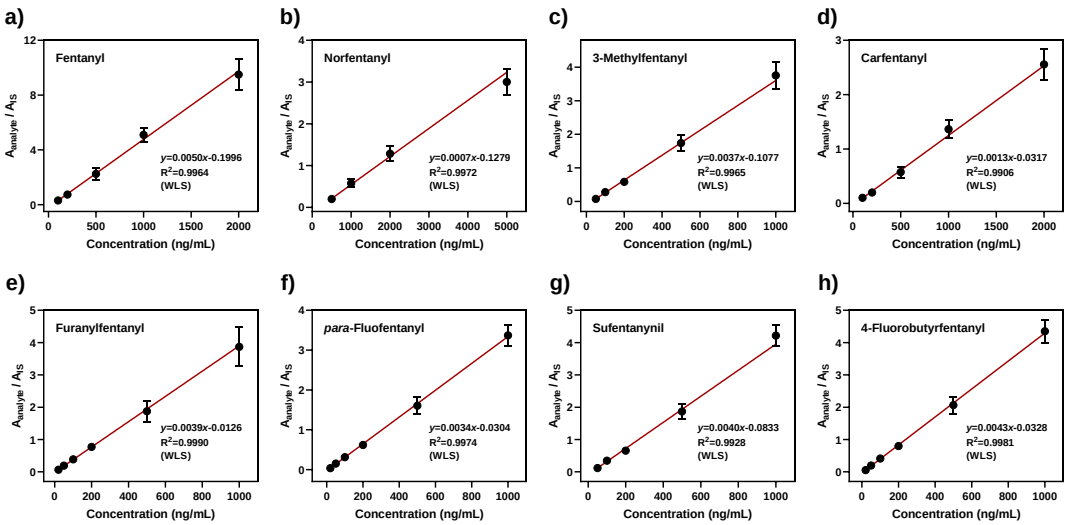

Fig. S8 Calibration curves of fentanyl (a), norfentanyl (b), 3-methylfentanyl (c), carfentanyl (d), furanylfentanyl (e), para-fluofentanyl (f), sufentanyl (g) and 4-fluorobutyrfentanyl (h).

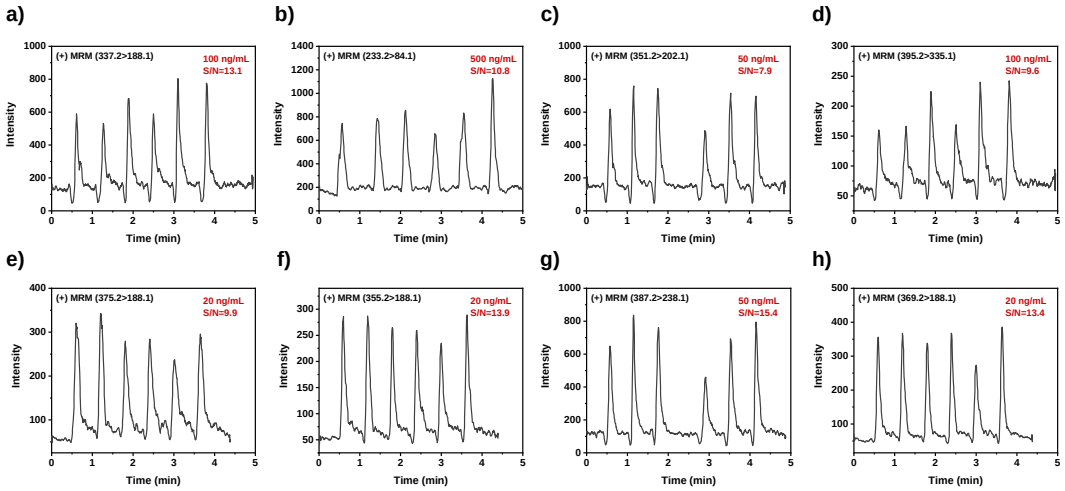

Fig. S9 Representative multiple-reaction monitoring chromatographs of quantified fentanyl (a), norfentanyl (b), 3-methylfentanyl (c), carfentanyl (d), furanylfentanyl (e), para-fluofentanyl (f), sufentanyl (g) and 4-fluorobutyrfentanyl (h).

a)

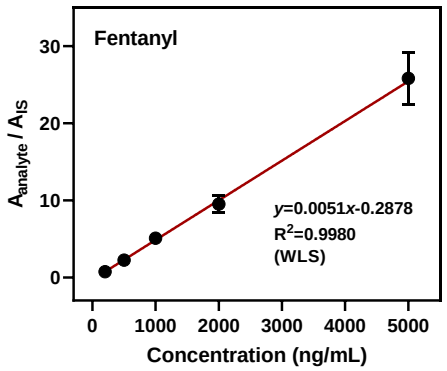

b)

Analyte	Detected (μg/mL)	
	Sample1	Sample2
Fentanyl	1.82 ± 0.23	3.51 ± 0.48

Fig. S10 Calibration curve of fentanyl for higher concentration quantification (a) and detected amounts in rat plasma samples (b). Sample1 was the rat plasma obtained by the tail vein injection of fentanyl at the dose of 3.1 mg/kg, and sample2 was that at the dose of 6.2 mg/kg.

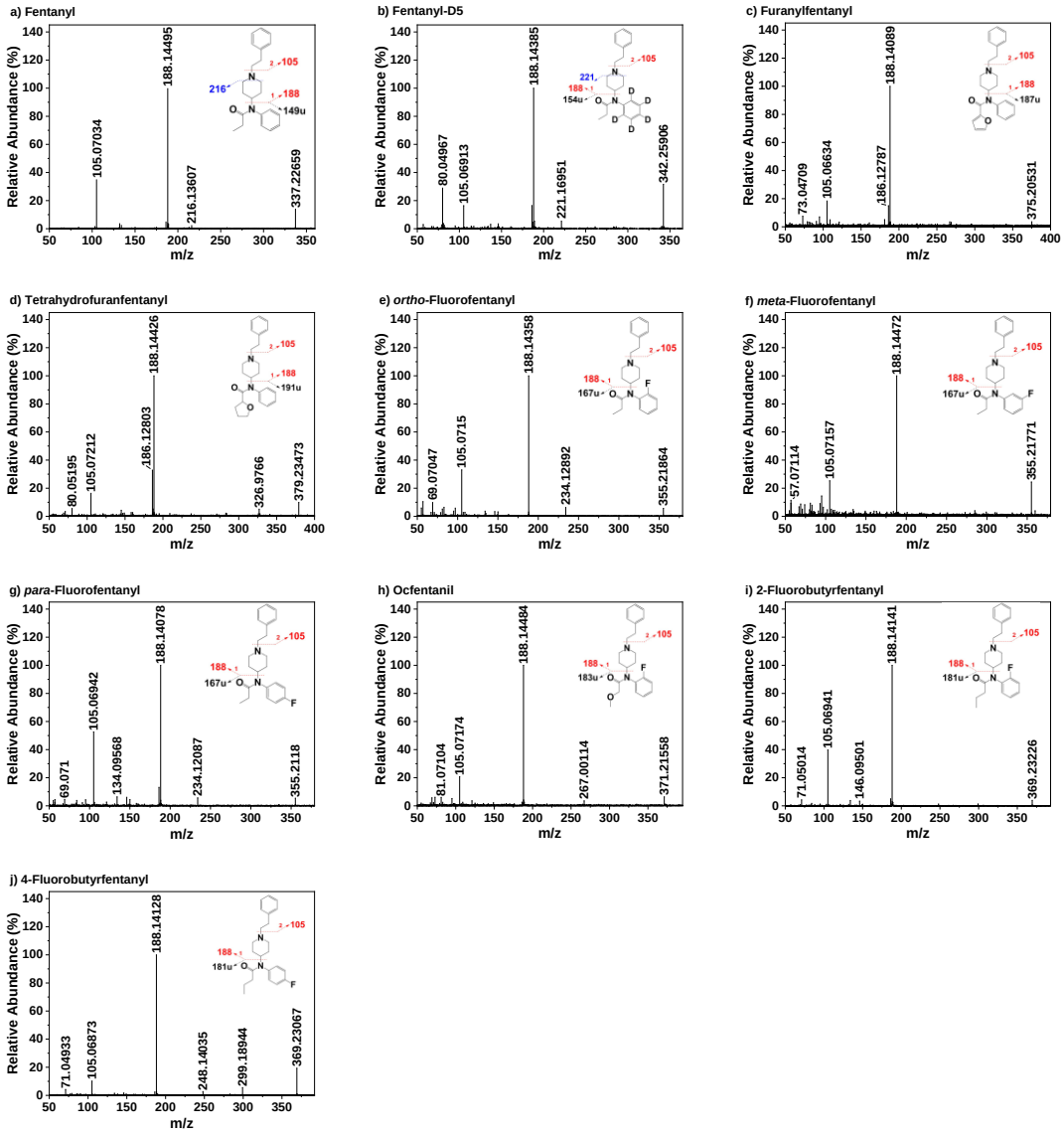

Fig. S11 DBDI-QTOF-MS/MS spectra of fentanyl (a); R3 modified furanylfentanyl (c) and tetrahydrofuranfentanyl (d); R4 modified fentanyl-D5 (b), *ortho*-fluorofentanyl (e), *meta*-fluorofentanyl (f), *para*-fluorofentanyl (g); R3+R4 modified ocfentanil (h), 2-fluorobutyrfentanyl (i) and 4-fluorobutyrfentanyl (j).

Two abundant product ions (m/z 188.1434 and 105.0699) were observed for fentanyl, fentanyl-D5, and R3, R4, R3+R4 modified FTNs, with the suggested fragmentation pathways for representative FTNs. The product ion at m/z 188.1434 was easy to form by cleavage of the N−piperidine ring bond between [R1+R2] and [R3+R4] moiety, leading to the elimination of [R3+R4] moieties as neutral losses (NL).

The m/z 188.1434 ion might also undergo a McLafferty rearrangement or be attributed to other isobaric product ions via different fragmentation pathways.[1,2] Another central product ion at m/z 105.0699 was assigned as a phenylethyl cation, resulting from the cleavage of the C−N bond between R1 and R2 moieties. Degradation of the piperidine ring may also form low abundance fragment ions such as m/z 216.1383. Characterized fragment ions at m/z 188.1434 and 105.0699 indicated that the modifications occur at R3 and R4 moieties, and the structures can be deduced along with the precursor ions and NL. The fixed precursor ion scan and NL scan could complement each other, jointly supporting the identification of R3, R4 and R3+R4 modified FTNs.

[1] X. Guo, Y. Shang, Y. Lv, H. Bai, Q. Ma, *Anal. Chem.*, 2021, **93**, 10152–10159.
[2] N. Qin, H. Wu, P. Xiang, B. Shen, J. Zhao, H. Deng, H. Qiang, F. Song, Y. Shi, *J. Am. Soc. Mass Spectrom.,* **2020**, 31, 277−291.

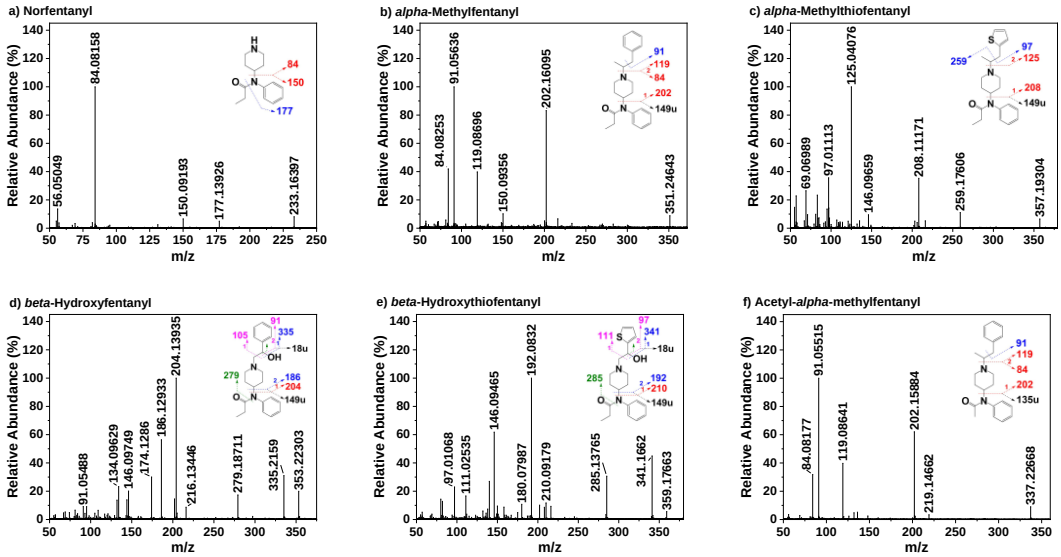

Fig. S12 DBDI-QTOF-MS/MS spectra of R1 modified *α*-methylfentanyl (b), *α*-methylthiofentanyl (c), *β*-hydroxyfentanyl (d), *β*-hydroxythiofentanyl (e); R1+R3 modified acetyl-*α*-methylfentanyl (f).

In the mass spectra of R1-modified FTNs, we did not observe product ions at m/z 188.1434 and 105.0699. Norfentanyl is a main non-reactive metabolite of fentanyl by cleavage of the piperidine ring N-dealkylation and is considered an R1-modified FTN here. Fragment ion at m/z 84.0808 was the most abundant product ion by [R1+R2]−[R3+R4] cleavage, and dissociation of the side chain at R3 moiety afforded low abundance product ion at m/z 177.1386. As α-methyl or β-hydroxyl substituted at the alkyl chain of R1, *e.g.*, α-methylfentanyl, α-methylthiofentanyl, β-hydroxyfentanyl, β-hydroxythiofentanyl and acetyl-α-methyl fentanyl, the abundant product ions were generated by [R1+R2]−[R3+R4] cleavage and R1−R2 cleavage. The cleavage between α- and β- bond of the alkyl chain, or dehydroxylation of β-hydroxyl formed the characterized fragmentation ions for these FTNs. Products ions at m/z 91.0564, 97.0111, and the dehydrated product ions of $[M-18]^+$ were helpful for the identification of α- and β- substituted R1 modified FTNs.

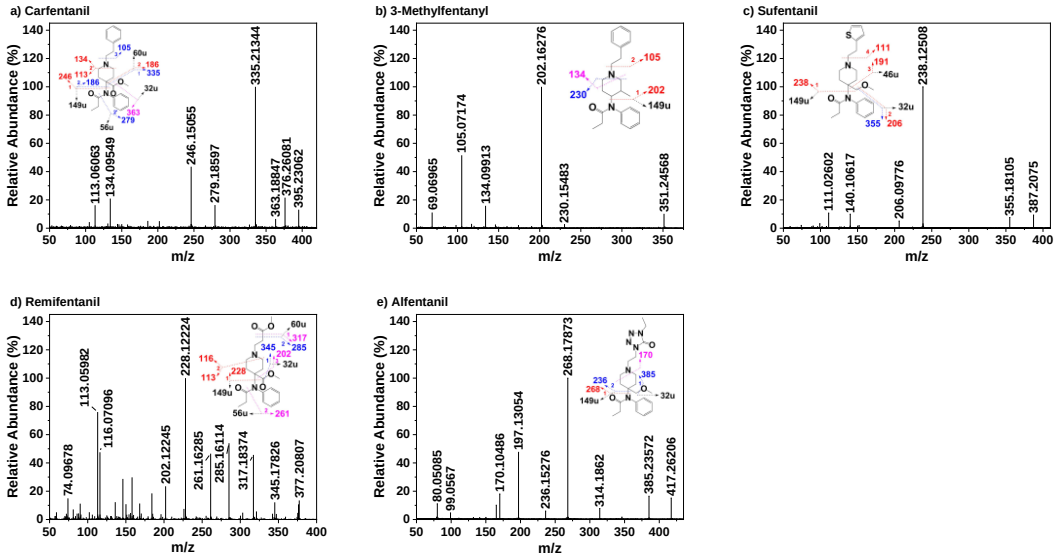

Fig. S13 DBDI-QTOF-MS/MS spectra of R2 modified carfentanil (a) and 3-methylfentanyl (b); R1+R2 modified sufentanil (c), remifentanil (d) and alfentanil (e).

Modifications of R2 moiety usually occurred at the 3- or 4- position of the piperidine ring. For 3-methylfentanyl as a methyl-substituted at position 3 of R2, abundant fragment ions at m/z 202.1590 and 105.0699 were produced the same way as fentanyl by [R1+R2]−[R3+R4] cleavage and R1−R2 cleavage. Substitution at position 4 of R2 changed the fragmentation pathways and generated more complicated fragmentations. For carfentanil, the most abundant product ion at m/z 335.2134 was attributed by cleavage of the ester-piperidine ring bond, followed by R3−R4 cleavage, [R1+R2]−[R3+R4] cleavage, and R1−R2 cleavage. Another fragmentation pathway was that [R1+R2]−[R3+R4] cleavage prioritized forming the product ion at m/z 246.1506, followed by cleavage of the ester-piperidine ring bond and the piperidine ring. Cleavage of ester bond-forming the fragment ion at m/z 363.1885 also occurred. Most fragment ions generated accompanying specific NL, e.g., m/z 363.1885 and 32 u (CH_4O), m/z 335.2134 and 60 u ($C_2H_4O_2$), m/z 279.1860 and 56 u (C_3H_4O), m/z 246.1506 and 149 u ($C_9H_{11}ON$). A similar fragmentation pathway was observed for sufentanil, remifentanil, and alfentanil. Product ions of $[M-32]^+$, $[M-56]^+$, $[M-60]^+$ and $[M-149]^+$ were noticeable for screening for these FTNs.

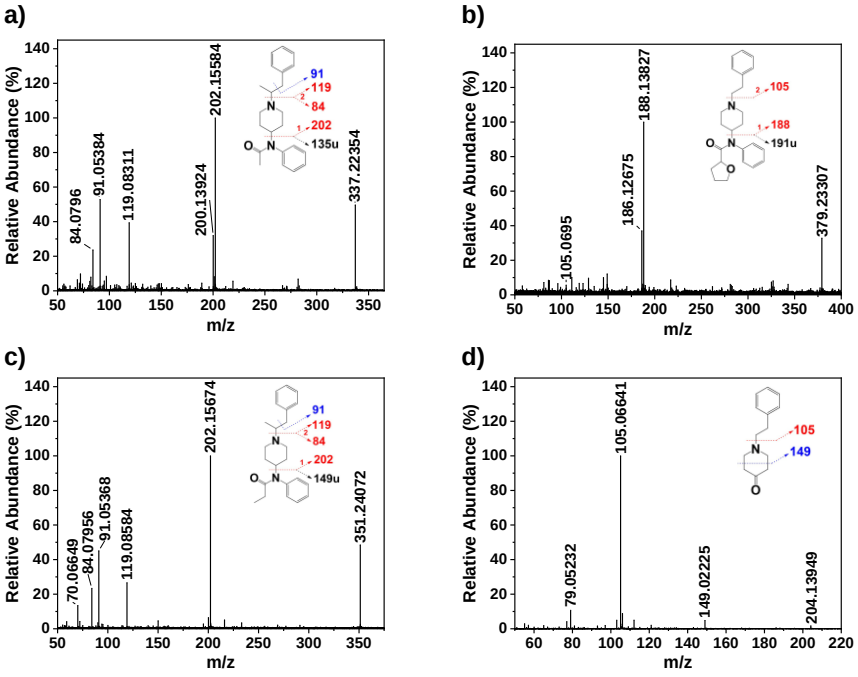

Fig. S14 DBDI-QTOF-MS/MS spectra of identified acetyl-α-methyl fentanyl (a) and tetrahydrofuranfentanyl (b) in random sample 3, α-methyl fentanyl (c) and N-phenethyl-4-piperidone (d) in random sample 4.

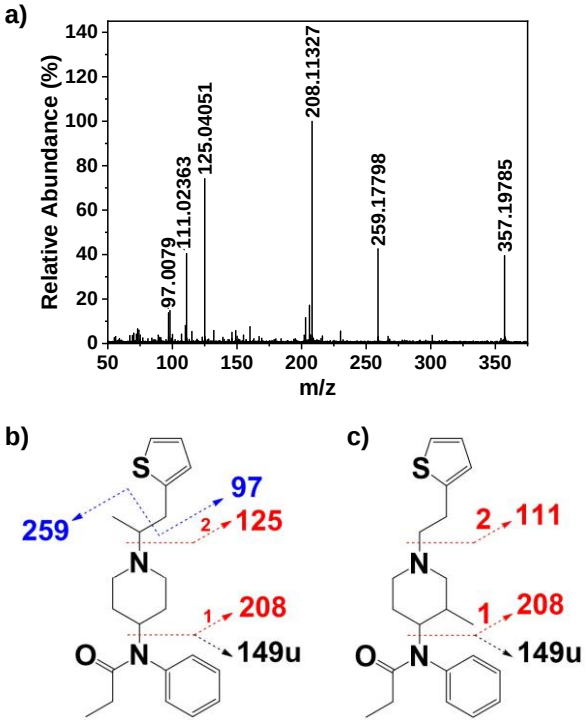

Fig. S15 DBDI-QTOF-MS/MS spectra of identified FTNs in random sample 5 (a) and structures of *α*-methylthiofentanyl (b) and 3-methylthiofentanyl (c).